Matter

Article

Multicomponent supramolecular nanoaggregates with co-emissive electrochemiluminescence

Graphical abstract

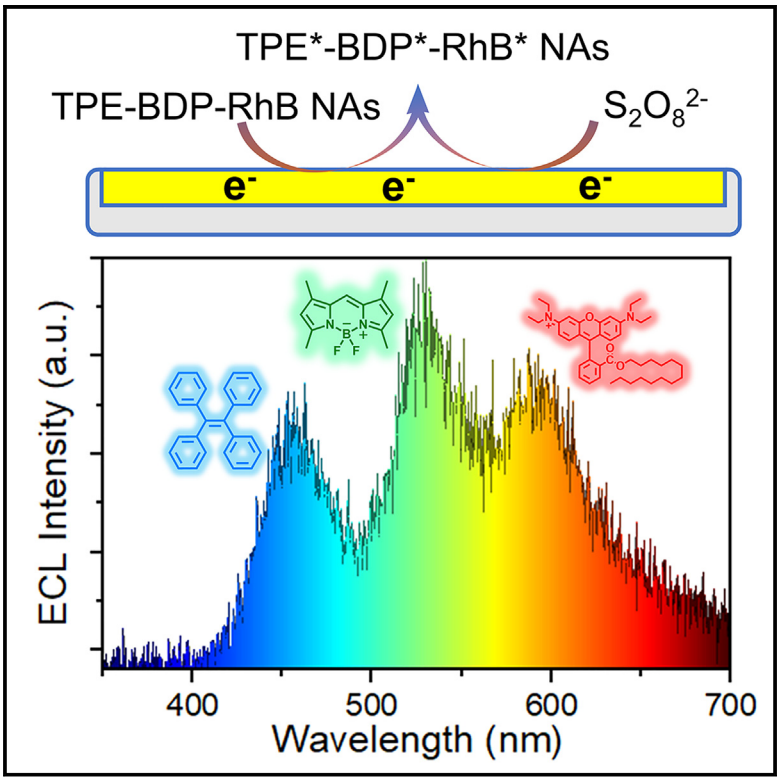

Highlights

- Small organic nanoaggregates in aqueous environment
- Synergistic supramolecular interactions of three components
- Co-emissive electrochemiluminescence (ECL) spanning entire visible light range
- Nanolabels for highly sensitive ECL immunoassays

Authors

Li Dai, Jinglong Fang, Tong Jiang, ..., Jianping Lei, Huangxian Ju, Qin Wei

Correspondence

liqi@ipe.ac.cn (Q.L.), chm_mahm@ujn.edu.cn (H.M.), chm_weiq@ujn.edu.cn (Q.W.)

In brief

Organic supramolecular nanoemitters show great promise in electrochemiluminescence (ECL). However, it is still a challenge to achieve excellent luminescent performances. Lipid-polymer (DSPE-PEG) encapsulated multicomponent nanoaggregates were prepared by employing microfluidic chips and were used as ECL nanolabels in immunoassays. Co-emissive ECL of three molecular components covering the full spectrum of visible light was achieved and higher ECL efficiency was obtained based on the synergistic supramolecular interactions.

Demonstrate
Proof-of-concept of performance with intended application/response

Dai et al., 2025, Matter *8*, 102056
June 4, 2025 © 2025 Elsevier Inc. All rights are reserved, including those for text and data mining, AI training, and similar technologies.
https://doi.org/10.1016/j.matt.2025.102056

CellPress

Please cite this article in press as: Dai et al., Multicomponent supramolecular nanoaggregates with co-emissive electrochemiluminescence, Matter (2025), https://doi.org/10.1016/j.matt.2025.102056

Matter

CellPress

Article

Multicomponent supramolecular nanoaggregates with co-emissive electrochemiluminescence

Li Dai,[1] Jinglong Fang,[1] Tong Jiang,[1] Qi Li,[2,3,*] Xiang Ren,[1] Yuyang Li,[1] Dan Wu,[1] Hongmin Ma,[1,5,*] Jianping Lei,[4] Huangxian Ju,[1,4] and Qin Wei[1,*]

[1]Key Laboratory of Interfacial Reaction & Sensing Analysis in Universities of Shandong, Collaborative Innovation Center for Green Chemical Manufacturing and Accurate Detection, School of Chemistry and Chemical Engineering, University of Jinan, Jinan 250022, China

[2]State Key Laboratory of Biochemical Engineering, Institute of Process Engineering, Key Laboratory of Biopharmaceutical Preparation and Delivery, Chinese Academy of Sciences, Beijing 100190, China

[3]University of Chinese Academy of Sciences, Beijing 100049, China

[4]State Key Laboratory of Analytical Chemistry for Life Science, School of Chemistry and Chemical Engineering, Nanjing University, Nanjing 210023, China

[5]Lead contact

*Correspondence: liqi@ipe.ac.cn (Q.L.), chm_mahm@ujn.edu.cn (H.M.), chm_weiq@ujn.edu.cn (Q.W.)

https://doi.org/10.1016/j.matt.2025.102056

PROGRESS AND POTENTIAL Electrochemiluminescence (ECL) is an advanced detection technique that overcomes key limitations of optical excitation techniques, including light scattering and autofluorescence. By eliminating these interferences, ECL achieves exceptionally sensitive detection, making it ideal for high-precision applications. ECL offers additional advantages through its simplified instrumentation, eliminating the need for monochromators or filters. The technique utilizes highly sensitive photomultiplier tubes to detect emitted light, where the entire emission spectrum contributes to the signal intensity. This unique feature allows the multicomponents of an aggregate system to contribute collectively to the ECL signal intensity. However, there are few reports on the development of multicomponent co-emissive ECL systems from this perspective. In the present work, three simple organic molecules with emissions located in the blue, green, and red regions were selected for the construction of nanoassemblies to demonstrate their spectrum contributions to ECL sensitivity. Co-emissions of these luminescent molecules in the form of supramolecular nanoaggregates were achieved under the same electrochemical excitation conditions. Synergistic enhancement effects of components for higher ECL efficiency were demonstrated, and the mutual supramolecular interactions were revealed. The proposed supramolecular strategies for organic nanoemitters may open new avenues for the development of nanotags for ECL immunoassays.

SUMMARY

The development of particulate electrochemiluminescence (ECL) emitter with high efficiency is challenging due to either the low electrochemical reaction efficiency for nanoparticles with larger sizes or the low quantum efficiency of molecular luminophores in aggregated forms. While the synthesis of aggregation-induced electrochemiluminescence (AI-ECL) luminophores with high quantum efficiency requires complicated procedures, a supramolecular strategy is proposed for constructing multicomponent nanoaggregates with co-emissive ECL. Aggregation-induced emission (AIE) active tetraphenylethylene (TPE) was used as a molecular matrix to disperse the aggregation-caused quenching (ACQ) luminophores with high quantum efficiency, boron dipyrromethene (BDP), and rhodamine B (RhB). Co-emissions of both molecular matrix and doped luminophores were achieved. The synergistic effects of the supramolecular interactions for enhancement of emission efficiency were confirmed by spectral measurement and molecular dynamic simulation. Small nanoaggregates with higher ECL efficiency were prepared on microfluidic chips and were used as nanolabels for sensitive ECL immunoassays.

 © 2025 Elsevier Inc. All rights are reserved, including those for text and data mining, AI training, and similar technologies.

Please cite this article in press as: Dai et al., Multicomponent supramolecular nanoaggregates with co-emissive electrochemiluminescence, Matter (2025), https://doi.org/10.1016/j.matt.2025.102056

INTRODUCTION

Electrochemiluminescence, also known as electrogenerated chemiluminescence (ECL), has found good application in clinical bioassays and shows promising potential in several new areas.[1–4] The exploitation of nanostructured materials as new generational emitters and substitutes to traditional molecular labels for sensitive immunoassays arouses the great enthusiasm of researchers because of the multi-label effect for signal amplification.[5,6] Various nanomaterials, such as quantum dots,[7] organic frameworks,[8–10] polymer dots,[11] carbon-based nanoparticles,[12] nanoclusters,[13] and molecular-doped nanoparticles,[14] have been well investigated for the development of ECL bioassays. However, the ill-defined structures, bad preparation reproducibility, high-energy surface induced nonspecific adsorption and other issues still challenge the extensive application of these nanosystems.

In comparison with inorganic nanomaterials, organic nanoparticles composed of small molecules have the advantages of well-defined structure, tunable wavelength, easy modification, and facile preparation.[15,16] Nanoprecipitation is a simple method for the preparation of organic nanoparticles from small organic building blocks.[17] However, the poor water dispersibility of organic nanoparticles depresses the ECL efficiency and hinders the application in aqueous solutions.[18] Amphiphilic polymers encapsulated nanoaggregates (NAs) not only address the issue of water dispersibility of organic molecules, but also avoid the molecular modification for bioconjugation.[19] These nanoassemblies have received great attention in the field of bioimaging and nanodrugs,[20,21] but seem at the initial stage for ECL application.[22] As an electrochemical stimulated emission process, ECL also suffers from the same problem of aggregation-caused quenching (ACQ) of organic nanoparticles with light-stimulated photoluminescences.[23] With the explosive development of aggregation-induced emission (AIE) technique, aggregation-induced electrochemiluminescence (AI-ECL) has been proposed and become a research focus in ECL application.[24–26]

Tetraphenylethylene (TPE) is one of the most simple AIE active molecules and can form nanocrystals with AI-ECL activity.[27] The ECL efficiency of TPE NAs in dispersible form is relatively low due to the small molecular size and weak restriction of intramolecular motions (RIM). Keeping step with the development of new AIE luminogens (AIEgens), great efforts have been made to the synthesis of complex derivatives with improved AI-ECL activity.[28–31] While the synthetic approaches require complicated procedures and are not cost-effective, little attention has been paid to the supramolecular strategies to improve the ECL behaviors of AIE molecules. Taking advantage of the unique electrochemical excitation mechanism of ECL, incorporation of multicomponent molecules or other types of units with different electrochemical behaviors into one system can afford potential-resolved or spectral-resolved multicolor probes for multivariate analysis.[32–34] However, there are few reports on the development of multicomponent co-emissive ECL systems for the improvement of ECL efficiencies. Although TPE has relatively lower AIE quantum efficiencies in the form of NAs, it can act as an excellent molecular matrix for loading of ACQ luminophores with high quantum efficiencies and can prevent the ACQ effect in NAs. The incorporation of different molecular luminophores with similar electrochemical behaviors can achieve the co-emissive ECL and synergistic effects for enhancement of ECL efficiency are expected.

In this work, multicomponent supramolecular NAs with TPE as a molecular matrix, boron dipyrromethene (BDP) as a high efficiency luminophore, and myristyl-modified rhodamine B (RhB) as a colloidal stabilizer were designed and co-emissive ECL of these components were achieved. Synergistic effects of mutual supramolecular interactions for enhancement of ECL efficiency were revealed. Continuous flow preparation methods on microfluidic chips in this work not only guarantee the batch reproducibility but also generate smaller NAs, which is beneficial for immunoassays in practical applications. The proposed supramolecular strategies for nanosystems with co-emissive ECL may open new avenues for development of nanoprobes for sensitive immunoassays.

RESULTS AND DISCUSSION

Preparation of multicomponent NAs on microfluidic chips

NAs of organic molecules are usually prepared by nanoprecipitation methods in which molecular precursors are dissolved in an organic solvent and then mixed with a miscible antisolvent.[29] This process produces larger organic nanoparticles with poor water dispersibility. The presence of lipids, amphiphilic polymers, or other surfactants in precursor solution can obviously reduce the particle size and enable good water dispersibility.[25] However, the organic nanoparticles prepared from this kinetically controlled process still suffer from wide size distribution and bad batch-to-batch reproducibility. These issues become worse in the case of preparation of multicomponent supramolecular NAs. Thus, polydimethylsiloxane (PDMS) microfluidic chips with fluidic focusing microreactors and different microchannel dimensions were adopted in this work to prepare multicomponent NAs in a continuous flow mode (Figure S1). A widely used lipid-polymer in drug delivery and bioimaging,[35] DSPE-PEG2k, was used to control the water dispersibility and encapsulate three organic molecules, TPE, BDP, and RhB (Figure 1A). Unless otherwise specified, the molecular NAs mentioned below were protected by this lipid-polymer.

Besides the single-component NAs of these molecules, two-component (TPE-BDP, TPE-RhB) and three-component (TPE-BDP-RhB) supramolecular NAs were also prepared on microfluidic chips under the same conditions. Here, TPE-BDP and TPE-BDP-RhB NAs were compared to present the typical morphologies and to demonstrate the advantages over conventional methods. In comparison with the NAs prepared using bulk nanoprecipitation methods, the microfluidic-prepared NAs show obviously reduced particle size and much narrower size distribution (Figures 1B and 1E). Moreover, the particle size of NAs can be tailored by the adjustment of microchannel dimension. With the reduction of microchannel dimension to 100 μm, small NAs with diameters of approximately 4.5 nm and 16.4 nm were obtained for TPE-BDP and TPE-BDP-RhB, respectively. Generally, the smaller

Please cite this article in press as: Dai et al., Multicomponent supramolecular nanoaggregates with co-emissive electrochemiluminescence, Matter (2025), https://doi.org/10.1016/j.matt.2025.102056

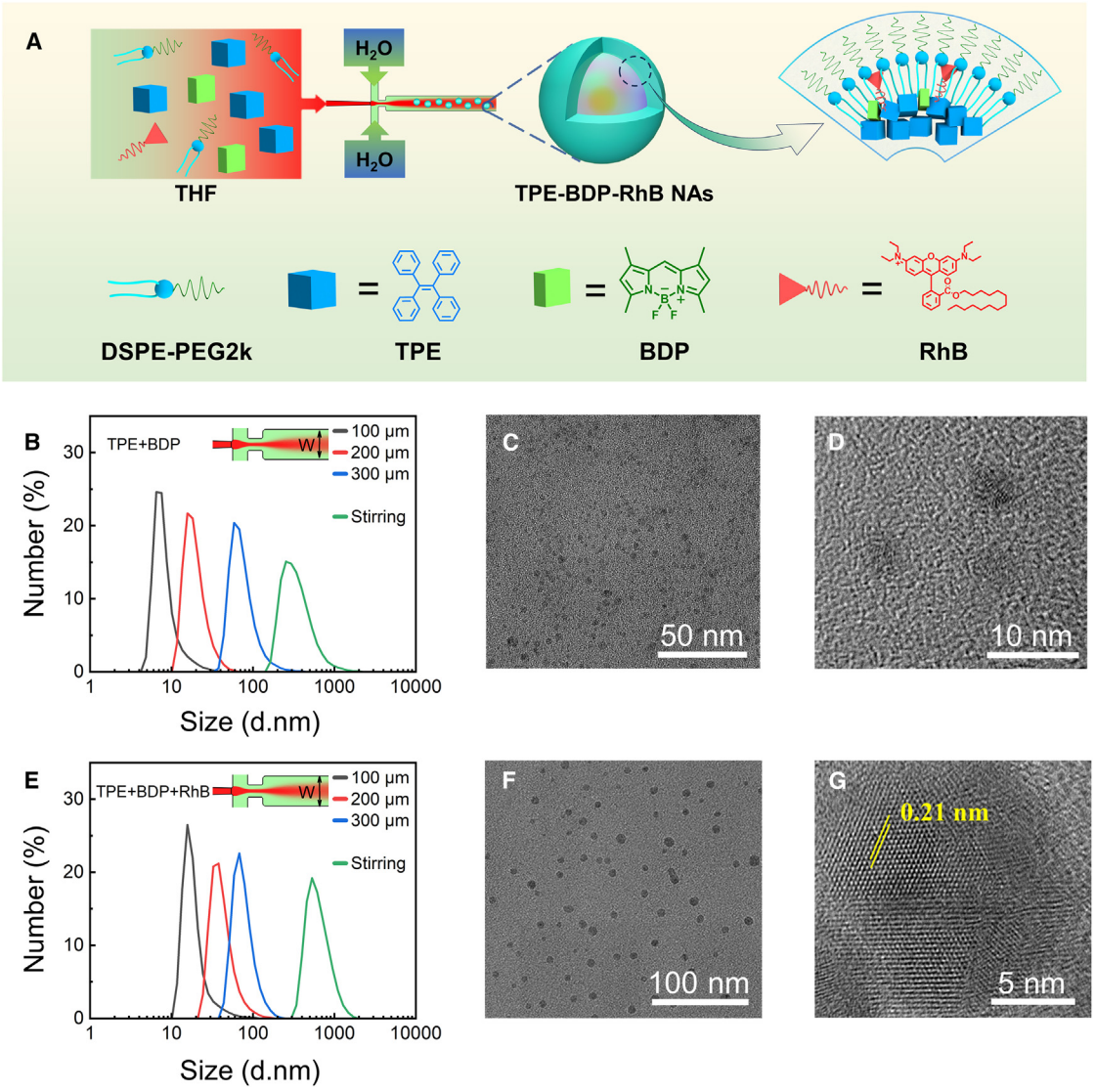

Figure 1. The preparation methods and characterization results of the multicomponent NAs

(A) Schematic diagram of the preparation of TPE-BDP-RhB NAs on microfluidic chips.

(B and E) The hydrodynamic size distributions of (B) TPE-BDP NAs and (E) TPE-BDP-RhB NAs under different preparation conditions (W: microchannel width of PDMS chip; stirring: prepared by precipitating without the use of PDMS chip).

(C, D, F, and G) TEM images of TPE-BDP NAs (C and D) and TPE-BDP-RhB NAs (F and G).

NAs at this scale are preferred for immunoassay and other biomedical applications.[20] Due to the effective mass transfer and fast kinetics of phase separation in microchannels, amorphous NAs are usually observed.[36] Only very small crystallization degree was observed for TPE-BDP NAs (Figure 1D). However, TPE-BDP-RhB NAs show higher crystallinity, which can be confirmed by both HR-TEM (Figure 1G) and the SAED (selected area electron diffraction) pattern (Figure S2). This indicates that the incorporation of RhB induces enhanced intermolecular actions. The myristyl-modified amphiphilic RhB not only enhances the supramolecular interactions but also improves the colloidal stability of TPE-BDP-RhB NAs, which are discussed blow.

Mutual supramolecular interactions and enhanced aggregation-induced emission

Three typical luminescent molecules with emissions located at blue (TPE), green (BDP), and red (RhB) regions were selected for construction of nanoassemblies with co-emissions covering the whole visible light range. AIE molecules are necessary candidates for preparation of molecular NAs while ACQ molecules have been rarely considered.[37] We demonstrate that the ACQ effects of BDP and RhB can be well inhibited after the incorporation into AIE molecular matrix of TPE. The hydrophobic modification of RhB with myristyl (Figure S3) does not alter the luminescent property in organic solvent (Figure S4) but induces strong ACQ effect in aqueous solution due to the change of solubility

Please cite this article in press as: Dai et al., Multicomponent supramolecular nanoaggregates with co-emissive electrochemiluminescence, Matter (2025), https://doi.org/10.1016/j.matt.2025.102056

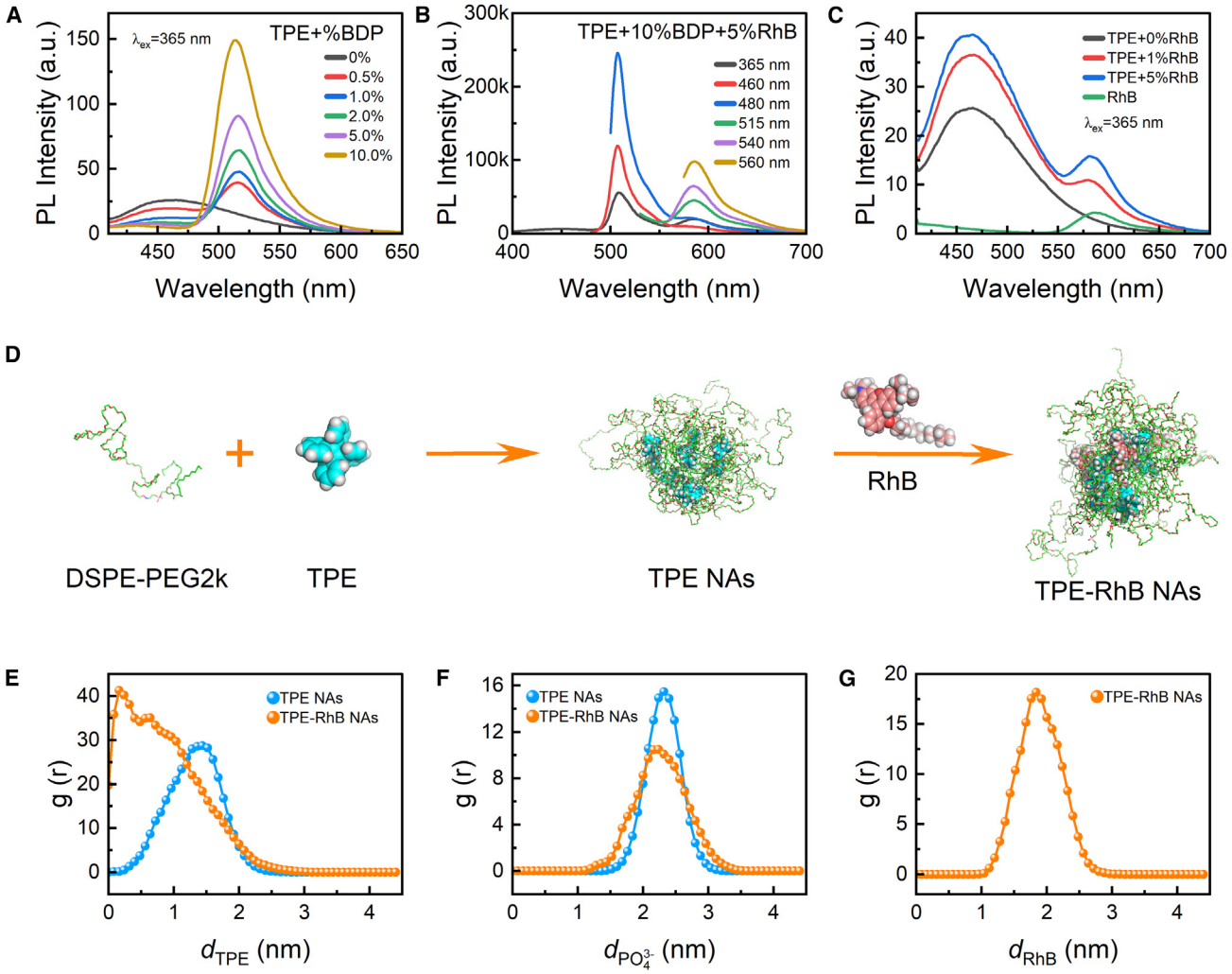

Figure 2. Characterizations of the intermolecular interactions by fluorescence spectra and molecular dynamics simulation

(A) The fluorescence spectra of TPE-BDP NAs prepared at various feeding mass ratios (TPE concentration: 1.0 mg/mL). The inset shows the change of the fluorescence colors with the naked eye.

(B) Fluorescence spectra of TPE-BDP-RhB NAs at different excitation wavelengths.

(C) The fluorescence spectra of TPE-RhB NAs prepared at various feeding mass ratios (TPE concentration: 1.0 mg/mL).

(D) Molecular dynamics simulation representation of TPE-RhB NAs.

(E–G) Radial distribution functions of the components around the hydrophobic core of TPE and TPE-RhB NAs: (E) TPE molecules, (F) the phosphate group on DSPE-PEG2k, and (G) RhB molecules.

and aggregation (Figure S5). This forms the prerequisite for co-encapsulation into NAs with other two hydrophobic molecules and indicates the amphiphilicity of the modified RhB. Before the discussion of intermolecular actions, the successful co-encapsulation of TPE, BDP, and RhB inside the prepared NAs can be confirmed by the changes of the transmembrane behaviors of these components and the co-localization imaging results of A549 cells, which can be found in Figure S6.

Figure 2A shows the fluorescence spectra of TPE NAs and TPE-BDP two-component NAs with different mass ratios of BDP/TPE in precursor solutions, while the TPE concentration was kept constant at 1 mg/mL. With the increase of BDP concentration, the broad AIE fluorescence emission of TPE located at 460 nm decreased gradually and the narrower fluorescence emission of BDP located at 515 nm emerged and increased sharply. The emission colors of the NA solutions under naked eyes also changed from blue to green (Figure S7). With the further increase of BDP concentration, the TPE emission almost disappears and the emission intensity at 515 nm begins to decrease (Figure S7). The disappearance of TPE emission easily can be attributed to the fluorescence resonant energy transfer (FRET) from TPE to BDP in consideration of the sufficient overlap between the emission spectrum of TPE and absorption spectrum of BDP (Figure S8). The decrease of BDP emission at high concentration can be attributed to the ACQ effect even under the double inhibiting effect of TPE and lipid matrix.[38] The

Please cite this article in press as: Dai et al., Multicomponent supramolecular nanoaggregates with co-emissive electrochemiluminescence, Matter (2025), https://doi.org/10.1016/j.matt.2025.102056

inhibiting effect of TPE matrix on ACQ can be further demonstrated by the fluorescence enhancement of BDP, while keeping the BDP concentration constant and increasing the concentration of TPE in NAs (Figure S9). The bathochromic shift of maximum emission wavelength and the broadening of peak width should be attributed to the simultaneous formation of both monomers and the J-aggregates of BDP in the matrix of TPE.[39] This can also explain the broader ECL spectrum of BDP in NAs, which will be discussed below. A maximum emission from BDP was achieved at a BDP/TPE ratio of 1:10, indicating that BDP should only be doped at low mass ratios.

The further incorporation of third component RhB into NAs can also achieve the co-emissions of three precursors, which can be reflected by the well-resolved emission bands of both BDP and RhB through the change of excitation wavelength (Figure 2B). While keeping the mass ratio of BDP/TPE at 1:10, RhB can also only be doped at low ratios due to the ACQ effects. The incorporation of RhB at ratios lower than 0.5:1:10 (RhB/BDP/TPE) shows little impact on BDP emission but can enhance the TPE emission (Figure S10), which almost disappears due to FRET from TPE to BDP. This indicates that the recovery of TPE emission at these ratios was not caused by the interruption of FRET between TPE and BDP. Under the excitation wavelength of both TPE (365 nm) and BDP (480 nm), only small fluorescence signals of RhB (580 nm) were observed (Figure 2B), indicating that only weak FRET between BDP and RhB occurred.

The enhancement effect of RhB inclusion on TPE emission can also be confirmed by the fluorescence investigation of TPE-RhB NAs with the increase of RhB/TPE mass ratio (Figure 2C). The weak fluorescence signals of RhB under the excitation wavelength of 365 nm also indicated the poor FRET between TPE and RhB. However, the fluorescence emission of RhB in TPE-BDP-RhB NAs under its own excitation wavelength (530 nm) was enhanced in comparison with RhB NAs (Figure S11), indicating the existence of the same TPE matrix inhibiting effect on RhB. The further increase of RhB/TPE ratio caused obviously depression of TPE emission and the RhB emission showed only small enhancement, which can be understood by the ACQ effect of RhB (Figure S12). The fluorescence lifetime of TPE molecules in TPE NAs and TPE-RhB NAs were measured and it changed from 3.7 ns to 5.1 ns (Figure S13), indicating the change of aggregation state of TPE molecules after the incorporation of RhB.To elucidate the supramolecular interactions in NAs, the aggregate structures of both TPE and TPE-RhB NAs were probed by molecular dynamic simulation (Figure 2D). For TPE NAs, TPE molecules are loosely encapsulated within the lipid matrix of DSPE-PEG2k. In contrast, for TPE-RhB NAs in the presence of RhB, the TPE molecules are aggregated in a more compact structure. The change of the aggregate structures can be further confirmed by the radial distribution functions (RDF) of TPE (Figure 2E), phosphate group on DSPE (Figure 2F), and RhB (Figure 2G) around the hydrophobic core of DSPE-PEG2k assemblies.

TPE molecules in TPE-RhB NAs are clearly more enriched in hydrophobic core than that in TPE NAs. The incorporation of RhB shows little impact on the position of phosphate group but the distribution becomes sharper (Figure 2E). This indicates that the micelle structure of DSPE-PEG2k becomes more ordered. RhB molecules are closer to the phosphate group and separated with the TPE domain (Figure 2G), which can be explained by the amphiphilic structure of RhB and the electrostatic interaction between the negatively charged phosphate group and positively charged RhB. The difference of zeta potential of these two NAs can confirm this electrostatic interaction (Figure S14). The amphiphilic RhB forms mixed micelle systems with DSPE-PEG2k and drives the TPE molecules concentrated in the hydrophobic core, forming a more compact structure. The change of aggregate state of TPE molecules explains not only the enhancement of AIE emission (Figure 2C) but also the more crystalized structure of TPE-BDP-RhB NAs (Figure 1G). The incorporation of RhB and the formation of electrostatic micelle interface also afford an improved long-term colloidal stability of TPE-BDP-RhB NAs over TPE-BDP NAs, which can be revealed by fluorescence monitoring (Figure S15) and the following ECL investigation.

After elucidating the supramolecular interactions of the components, the fluorescence quantum yields (PLQY) of the NAs with different preparation conditions were calculated and compared (Figure S16; Table S1). It should be noted that, due to the existence of multicomponents and the overlying of absorption, the calculated PLQY of multicomponent NAs depend on the excitation wavelengths. In consideration of the dominating emission roles of BDP and the enhancement effects of molecular matrix discussed above, the PLQY of BDP and TPE-BDP NAs were calculated at the excitation wavelength of 470 nm, which ensures a whole emission profile of BDP. A very high PLQY (0.97) was obtained for TPE-BDP NAs, indicating the good dispersion ability and ACQ inhibiting effects of TPE matrix. To cover all the emission bands for TPE-BDP-RhB NAs, a short excitation wavelength of 365 nm was used and a relatively lower PLQY (0.93) was obtained due to the lower quantum efficiency of TPE. For the influences of aggregate sizes, higher PLQY was obtained for smaller NAs.

Co-emissive ECL of TPE-BDP-RhB NAs

In accompaniment with the fluorescence investigation, the ECL behaviors of single-component TPE NAs and multicomponent NAs (TPE-BDP, TPE-BDP-RhB) with different component ratios were compared under the co-reaction system of $K_2S_2O_8$. The chemical routes of $K_2S_2O_8$ co-reaction system for the generation of cathodic ECL signals have been well exploited.[40] All three molecules (TPE, BDP, and RhB) show reduction waves during cathodic potential scans (Figure S17) and thus can produce radical anions. The formation of sulfate radical anion ($SO_4^{\cdot -}$) during cathodic potential scans can act as a strong oxidant and react with the radical anion of luminophore to produce an emissive excited state (Figure 3A). The ECL spectra of the single-component NAs match well with their corresponding fluorescence spectra (Figure S18), indicating the generation of similar excited states of these molecules. The maximum ECL signals of these NAs were achieved at the highest potential (−1.6 V) within the scanning range (Figure 3B). With repeated potential scans, reproducible transient signals can also be recorded against time for quantitative comparison (Figure 3C). Compared with TPE NAs, TPE-BDP NAs show greatly enhanced ECL emissions after the incorporation of BDP (Figure 3D). The ECL

Please cite this article in press as: Dai et al., Multicomponent supramolecular nanoaggregates with co-emissive electrochemiluminescence, Matter (2025), https://doi.org/10.1016/j.matt.2025.102056

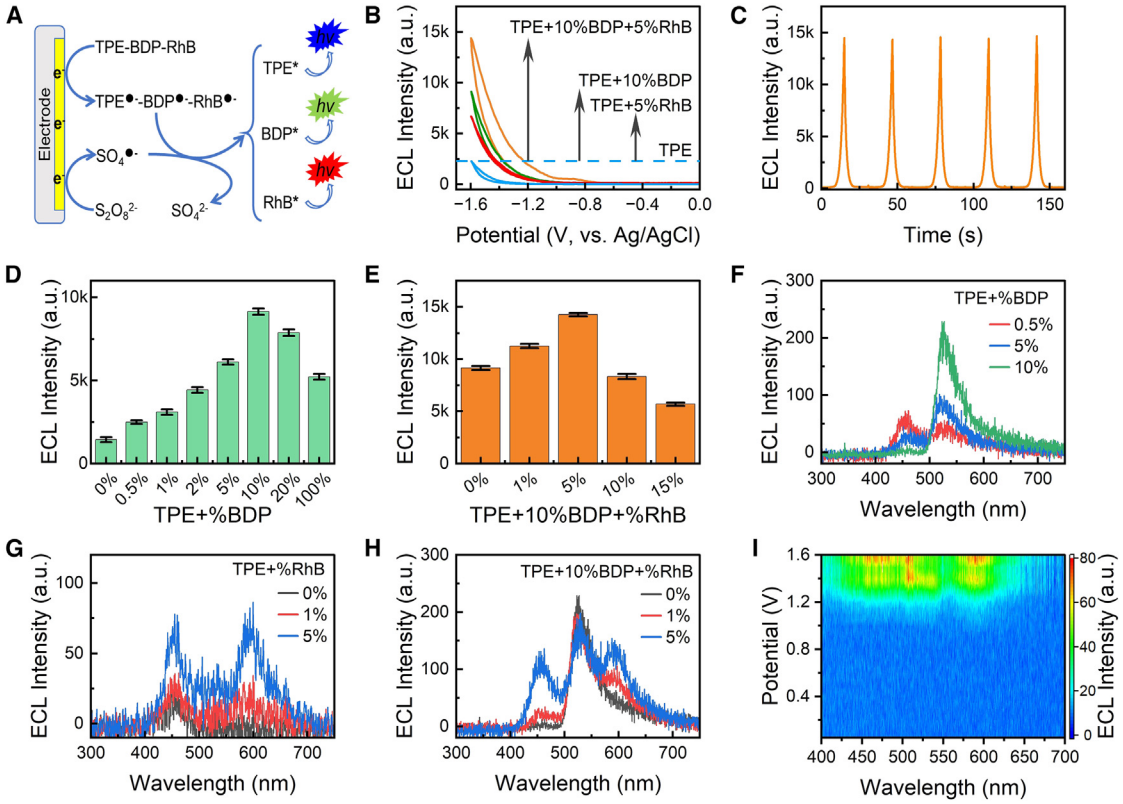

Figure 3. The ECL behaviors of the multicomponent NAs

(A) The chemical routes of TPE-BDP-RhB NAs for generation of ECL.

(B) ECL-potential curves of TPE NAs, TPE-BDP NAs, TPE-RhB NAs, and TPE-BDP-RhB Nas.

(C) ECL-time curves of TPE-BDP-RhB NAs. Condition: PBS solution including 80 mM $K_2S_2O_8$, pH 7.4.

(D) The optimization of the loading ratios of BDP in TPE-BDP NAs (TPE concentration: 1.0 mg/mL).

(E) The optimization of the loading ratios of RhB in TPE-BDP-RhB NAs (TPE:BDP=10:1).

(F) ECL spectra of TPE-BDP NAs with varying BDP ratios.

(G) ECL spectra of TPE-RhB NAs with varying RhB ratios.

(H) ECL spectra of TPE-BDP-RhB NAs with varying RhB ratios.

(I) Potential-resolved ECL spectrum of TPE-BDP-RhB NAs (vs. Ag/AgCl).

Error bars: the standard deviation (SD) of 5 independent measurements.

emission of TPE-BDP-RhB NAs are further enhanced significantly with the inclusion of RhB (Figure 3E). Higher doping ratios of BDP and RhB also cause decrease of ECL intensity. The turning points on ECL intensity of both TPE-BDP and TPE-BDP-RhB NAs occur at the same mass ratios (1:10 and 0.5:1:10 for BDP/TPE and RhB/BDP/TPE, respectively) as that for fluorescence investigation. This consistence indicates the same molecular basis of component interactions on fluorescence and ECL emissions.

To further confirm the supramolecular interactions during ECL emissions, the ECL spectra of NAs with different components and doping ratios were collected. For TPE-BDP NAs with increase of BDP doping ratios, the BDP emission band become dominant and the weak emission band of TPE disappears gradually (Figure 3F). This change can also confirm the energy transfer from TPE to BDP during ECL emission. The enhancement effects of RhB inclusion on AI-ECL of TPE can be confirmed by ECL spectra of both TPE-RhB and TPE-BDP-RhB NAs (Figures 3G and 3H), where the emission at the blue light region obviously enhanced. Different from the fluorescence co-emission system, which the components should be excited at different wavelengths, the ECL co-emissions of components can be achieved under the same electrochemical excitation condition.[41] Three comparable emission bands located at blue, green, and red regions for TPE-BDP-RhB NAs confirm the co-emissive ECL of the components. The emissions of each component at different light regions undoubtedly contribute to the ECL signal that was recorded by PMT across the whole spectrum. However, the ECL intensity used for comparison was measured by the maximum transient signal, that is, the ECL intensity at the highest potential. The potential-resolved ECL spectra (Figure 3I) of TPE-BDP-RhB NAs reveal that this broad spectrum was achieved at more negative excitation potentials (<−1.0V) and maintained at the potential at which the ECL intensity was measured for comparison and quantification (−1.6V). This confirmed that the emission bands of three components all

Please cite this article in press as: Dai et al., Multicomponent supramolecular nanoaggregates with co-emissive electrochemiluminescence, Matter (2025), https://doi.org/10.1016/j.matt.2025.102056

Table 1. Evaluation of ECL efficiency of nanoparticles prepared with different microchannel dimensions

Microchannel dimension	100 μm	200 μm	300 μm	Stirring
TPE-BDP NAs	3.08	1.94	1.54	1[a]
TPE-BDP-RhB NAs	3.75	2.27	1.39	0.80

[a]Reference value, set as 1 for comparison.

contribute to the transient ECL intensity. Besides the measured ECL intensity, the ECL efficiency of the co-emissive NAs prepared with different microchannel dimensions were also calculated (Figures S19 and S20). As expected, higher ECL efficiency was observed for smaller NAs (Table 1).

Multicomponent NAs as ECL signal tags for immunoassays

While the prepared multicomponent NAs can produce enhanced ECL emissions on electrodes, they were exploited as signal tags for ECL immunoassays. The selection of functional group terminated DSPE-PEG2k can easily form conjugates with detection antibodies. The nanostructured TiO_2 (preparation and characterization details are presented in Figures S21–S24) were used as platforms for the immobilization of capturing antibodies. The construction details and the detection mechanism of the ECL immunoassays are depicted in Figure S25. The successful construction of sensing interface and the recognition ability toward a protein biomarker CD44 were confirmed by electrochemical characterizations (Figure S26). The experimental conditions for CD44 detection were also optimized based on the ECL measurement (Figure S26).

To demonstrate the superiority of NAs with higher ECL efficiency, both TPE-BDP NAs and TPE-BDP-RhB NAs were used as signal labels and the cathodic ECL intensities were correlated with the concentration of CD44 in standard solutions. While both bioassays show positive linear correlation in a broad concentration range (1 pg/mL to 200 ng/mL with TPE-BDP NAs and 0.5 pg/mL to 200 ng/mL with TPE-BDP-RhB NAs), the ECL response using the TPE-BDP-RhB NAs shows higher sensitivity (Figure 4A red line). The calculated limit of detection (LOD) decreased from 0.37 pg/mL (TPE-BDP NAs) to 0.18 pg/mL (TPE-BDP-RhB NAs), which is among the lowest in reported biosensors (Table S2). Besides the sensitivity improvement, TPE-BDP-RhB NAs also show superiority in storage stability of the constructed immunosensors over TPE-BDP NAs (Figure 4B). The small size, good water dispersibility, and the surface PEG layers with antifouling properties of labeling NAs can reduce the nonspecific adsorption on electrodes. Benefiting from this property, the proposed immunoassays also showed good selectivity toward CD44 and anti-interference capability toward several common protein biomarkers (Figure 4C). The application of supramolecular NAs to sensitive immunoassay holds promising potential for tremendous development.

Conclusion

A multicomponent nanoemitter with the co-emissive ECL was reported for the development of highly sensitive immunoassay signal tags. To overcome the ACQ effects that strongly influence the emission efficiency of the luminophores in particulate form, a supramolecular strategy combining the AIE molecular matrix and ACQ luminophores with high quantum efficiency was proposed. The high quantum efficiency of the ACQ luminophores could be reserved by controlling the mass ratios. Higher ECL efficiency was achieved for small NAs based on the supramolecular interactions. In consideration of the diversity of both AIE and ACQ molecules, this strategy deserves to be a versatile method for construction of co-emissive ECL nanoemitters. Co-emissive NAs with higher ECL efficiency also have promising potentials in development of highly sensitive clinical immunoassays.

METHODS

Materials and instruments

Boron dipyrromethene (BDP), tetraphenylethylene (TPE), rhodamine B (RhB), 1-tetradecanol, sulfoxide, dichloromethane, tetrabutyl titanate, (3-Aminopropyl) triethoxysilane (APTES), and potassium persulfate were purchased from Macklin Biochemical Co., Ltd. (Shanghai, China). DSPE-PEG2k and DSPE-PEG2k-COOH were purchased from Yusi Pharmaceutical Technology Co., Ltd. (Chongqing, China). Tetrahydrofuran, anhydrous ethanol, and ethylene glycol were purchased from Fuyu Fine Chemical Co., Ltd. (Tianjin, China). Column chromatography silica gel (particle size: 200–300 mesh) was purchased from the Qingdao Haiyang Chemical Co., Ltd (Qingdao, China). SU-8 2050 photoresist was purchased from KAYAKU Advanced Materials Inc. (USA), and polydimethylsiloxane (PDMS RTV615) was obtained from Momentive Performance Materials Inc. (USA). The antigen of CD44, capture-antibody (Ab_1), detection antibody (Ab_2), and antigens of PSA, HIg, CEA, AFP, and glucose were all purchased from Shanghai Linc-Bio Science Co. Ltd. (Shanghai, China). Bovine serum albumin (BSA) (96%–99%) was purchased from Sigma-Aldrich Co., Ltd. (St. Louis, MO, USA). All the other chemicals and reagents were purchased from commercial sources and used as received without further purification. The ultrapure water was obtained from the UP ultrapure water purification system.

The ^{1}H NMR was employed for characterization using the Avance III 400 MHz instrument by Bruker Biospin AG in Switzerland. Fluorescence spectra were measured using the PerkinElmer LS55 Fluorescence Spectrometer or the TECAN Spark Microplate Reader. UV-Vis absorption spectra were recorded on UV2550PC (Shimadzu, Japan). Electrochemical impedance spectra (EIS) was performed using an electrochemical workstation (Zahner Zennium PP211, Germany). Transmission electron microscopy (TEM) was conducted on a JEOL transmission electron microscope (JEM-2100F) at an acceleration voltage of 100 kV. Dynamic light scattering (DLS) and Zeta potential measurements were taken using an Anton Paar particle analyzer (Litesizer 500). The electrochemiluminescence (ECL) spectra were collected using the Guochen GCFG-B ECL spectrometer (Jinan, China). The fluorescence images of the cells were acquired using the Carl Zeiss (Shanghai, China) laser scanning confocal microscope (LSM880). X-ray diffraction (XRD) patterns was performed

Please cite this article in press as: Dai et al., Multicomponent supramolecular nanoaggregates with co-emissive electrochemiluminescence, Matter (2025), https://doi.org/10.1016/j.matt.2025.102056

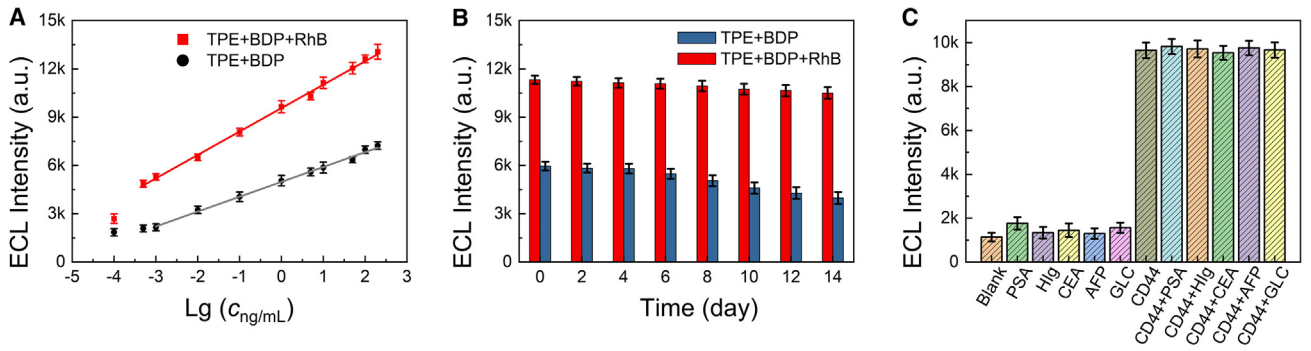

Figure 4. The sensing performances of the multicomponent NAs

(A) Calibration plot of immunosensors using TPE-BDP-RhB NAs and TPE-BDP NAs as signal labels at different CD44 concentrations (0.1 pg/mL to 200 ng/mL).

(B) Stability of immunosensor with 10 ng/mL of CD44 within 14 days.

(C) Specificity of immunosensor based on TPE-BDP-RhB NAs with 1 ng/mL of CD44 and 5 ng/mL of PSA, HIg, CEA, AFP, and GLC.

Error bars: the standard deviation (SD) of 5 independent measurements.

with D8 advance X-ray diffractometer (Bruker AXS, Germany). Fluorescence lifetime characterization was performed using Steady State and Transient State Fluorescence Spectrometer (FLS1000) from Edinburgh Instruments (United Kingdom). The electrochemical signals were collected using the CHI 660E electrochemical workstation. The electrochemiluminescence (ECL) measurements were performed on MPI-1 ECL analyzer (Remax, China).

Device fabrication and its implementation

The cross-shaped fluid-focusing microfluidic chip used in this study was fabricated using soft lithography techniques. Detailed information on the fabrication process and the chip's structural design can be found in the supporting information.

Hydrophobic modification of rhodamine B

Rhodamine B was hydrophobically modified through an esterification reaction using concentrated sulfuric acid as a catalyst, yielding a product with an 83% yield. Detailed experimental procedures and the ^{1}H NMR and fluorescence spectra of the product are available in the supplemental information.

Preparation of NAs

Figure 1A presents a schematic illustration of the preparation process. Nanoparticles were synthesized using a microfluidic chip equipped with fluid-focusing technology. The chip was designed with intersecting microchannels, enabling the central stream (containing the nanoparticle precursor solution) to be focused by two outer sheath flows. By precisely adjusting the flow rates of the sheath fluids relative to the central stream, as well as the composition of the precursor solution, the composition and size of the nanoparticles were precisely controlled. As the precursor solution passed through the focused region, a self-assembly process occurred, resulting in the formation of uniformly sized nanoparticles, which were collected at the outlet of the microfluidic chip. The produced nanoparticles were characterized for size, shape, and surface charge using techniques such as dynamic light scattering, transmission electron microscopy, and zeta potential analysis. Detailed information on the concentrations, flow rates, and characterization results of the nanoparticles can be found in the supplemental information.

ECL experimental system

In this study, an electrochemiluminescence (ECL) system was utilized for the quantitative detection of the target analyte, offering high sensitivity and minimal background interference. The ECL setup consisted of an electrochemical workstation (CHI660E), which provided the current and voltage signals necessary for electrochemical triggering. The ECL measurements were conducted using two complementary detection methods: ECL intensity monitoring with a photomultiplier tube (PMT) detector and spectral measurements with a charge-coupled device (CCD) detector.

The PMT operated under a negative high-voltage mode (−800 V) for enhanced sensitivity, while the CCD was maintained at a temperature of −65°C to reduce noise. The integration time for the CCD was adjusted according to the luminescence intensity, ranging from 0.1 to 100 s. The electrochemical measurements were carried out in a three-electrode system comprising a glassy carbon electrode (GCE) or gold electrode (GE) as the working electrode, a platinum wire as the counter electrode, and an Ag/AgCl electrode as the reference electrode. All measurements were conducted in a dark-room to minimize ambient light interference during electrochemical triggering and signal acquisition.

The data recorded by the PMT and CCD detectors were processed and analyzed using Origin software to extract meaningful results.

RESOURCE AVAILABILITY

Lead contact

Further information and requests for resources and reagents should be directed to and will be fulfilled by the lead contact, Hongmin Ma (chm_mahm@ujn.edu.cn).

Materials availability

This study did not generate new unique materials.

Data and code availability

All data generated during the study are available from the lead contact upon reasonable request. This study did not generate a code.

ACKNOWLEDGMENTS

This work was financially supported by the National Natural Science Foundation of China (22374059, 22274062) and the National Key R&D Plan of China (2023YFC3904601). H.M. thanks the Young Taishan Scholars Program of Shandong Province of China.

AUTHOR CONTRIBUTIONS

Conceptualization, H.M.; methodology, L.D. and H.M.; investigation, L.D. and T.J.; validation, J.F.; writing – original draft, L.D. and H.M.; writing – review and editing, Q.L. and J.L.; resources, X.R., Y.L., and D.W.; funding acquisition, H.M., Q.L., and Q.W.; supervision, H.J. and Q.W.

DECLARATION OF INTERESTS

The authors declare no competing interests.

SUPPLEMENTAL INFORMATION

Supplemental information can be found online at https://doi.org/10.1016/j.matt.2025.102056.

Received: August 12, 2024
Revised: December 27, 2024
Accepted: February 24, 2025
Published: March 19, 2025

REFERENCES

1. Wei, Y., Qi, H., and Zhang, C. (2023). Recent advances and challenges in developing electrochemiluminescence biosensors for health analysis. Chem. Commun. *59*, 3507–3522. https://doi.org/10.1039/d2cc06930j.
2. Gao, X., Jiang, G., Gao, C., Prudnikau, A., Hübner, R., Zhan, J., Zou, G., Eychmüller, A., and Cai, B. (2023). Interparticle Charge-Transport-Enhanced Electrochemiluminescence of Quantum-Dot Aerogels. Angew Chem. Int. Ed. Engl. *62*, e202214487. https://doi.org/10.1002/anie.202214487.
3. Meng, C., Knežević, S., Du, F., Guan, Y., Kanoufi, F., Sojic, N., and Xu, G. (2022). Recent advances in electrochemiluminescence imaging analysis. eScience *2*, 591–605. https://doi.org/10.1016/j.esci.2022.10.004.
4. Zhu, W., Dong, J., Ruan, G., Zhou, Y., and Feng, J. (2023). Quantitative Single-Molecule Electrochemiluminescence Bioassay. Angew Chem. Int. Ed. Engl. *62*, e202214419. https://doi.org/10.1002/anie.202214419.
5. Du, F., Chen, Y., Meng, C., Lou, B., Zhang, W., and Xu, G. (2021). Recent advances in electrochemiluminescence immunoassay based on multiple-signal strategy. Curr. Opin. Electrochem. *28*, 100725. https://doi.org/10.1016/j.coelec.2021.100725.
6. Fiorani, A., Merino, J.P., Zanut, A., Criado, A., Valenti, G., Prato, M., and Paolucci, F. (2019). Advanced carbon nanomaterials for electrochemiluminescent biosensor applications. Curr. Opin. Electrochem. *16*, 66–74. https://doi.org/10.1016/j.coelec.2019.04.018.
7. Yu, S., Du, Y., Niu, X., Li, G., Zhu, D., Yu, Q., Zou, G., and Ju, H. (2022). Arginine-modified black phosphorus quantum dots with dual excited states for enhanced electrochemiluminescence in bioanalysis. Nat. Commun. *13*, 7302. https://doi.org/10.1038/s41467-022-35015-9.
8. Qin, X., Zhan, Z., and Ding, Z. (2023). Progress in electrochemiluminescence biosensors based on organic framework emitters. Curr. Opin. Electrochem. *39*, 101283. https://doi.org/10.1016/j.coelec.2023.101283.
9. Mohan, B., Kumar, S., Kumar, V., Jiao, T., Sharma, H.K., and Chen, Q. (2022). Electrochemiluminescence metal-organic frameworks biosensing materials for detecting cancer biomarkers. TrAC-Trend. Anal. Chem. *157*, 116735. https://doi.org/10.1016/j.trac.2022.116735.
10. Wang, Y., Zhao, G., Chi, H., Yang, S., Niu, Q., Wu, D., Cao, W., Li, T., Ma, H., and Wei, Q. (2021). Self-Luminescent Lanthanide Metal-Organic Frameworks as Signal Probes in Electrochemiluminescence Immunoassay. J. Am. Chem. Soc. *143*, 504–512. https://doi.org/10.1021/jacs.0c12449.
11. Wang, N., Wang, Z., Chen, L., Chen, W., Quan, Y., Cheng, Y., and Ju, H. (2019). Dual resonance energy transfer in triple-component polymer dots to enhance electrochemiluminescence for highly sensitive bioanalysis. Chem. Sci. *10*, 6815–6820. https://doi.org/10.1039/c9sc01570a.
12. Ji, J., Wen, J., Shen, Y., Lv, Y., Chen, Y., Liu, S., Ma, H., and Zhang, Y. (2017). Simultaneous Noncovalent Modification and Exfoliation of 2D Carbon Nitride for Enhanced Electrochemiluminescent Biosensing. J. Am. Chem. Soc. *139*, 11698–11701. https://doi.org/10.1021/jacs.7b06708.
13. Zhou, Y., Chen, S., Luo, X., Chai, Y., and Yuan, R. (2018). Ternary Electrochemiluminescence Nanostructure of Au Nanoclusters as a Highly Efficient Signal Label for Ultrasensitive Detection of Cancer Biomarkers. Anal. Chem. *90*, 10024–10030. https://doi.org/10.1021/acs.analchem.8b02642.
14. Zanarini, S., Rampazzo, E., Bonacchi, S., Juris, R., Marcaccio, M., Montalti, M., Paolucci, F., and Prodi, L. (2009). Iridium Doped Silica−PEG Nanoparticles: Enabling Electrochemiluminescence of Neutral Complexes in Aqueous Media. J. Am. Chem. Soc. *131*, 14208–14209. https://doi.org/10.1021/ja906666e.
15. Xing, P., and Zhao, Y. (2016). Multifunctional Nanoparticles Self-Assembled from Small Organic Building Blocks for Biomedicine. Adv. Mater. *28*, 7304–7339. https://doi.org/10.1002/adma.201600906.
16. Qi, H., and Zhang, C. (2022). Organic nanoparticles for electrogenerated chemiluminescence assay. Curr. Opin. Electrochem. *34*, 101023. https://doi.org/10.1016/j.coelec.2022.101023.
17. Tian, F., Cai, L., Liu, C., and Sun, J. (2022). Microfluidic technologies for nanoparticle formation. Lab Chip *22*, 512–529. https://doi.org/10.1039/d1lc00812a.
18. Omer, K.M., and Bard, A.J. (2009). Electrogenerated Chemiluminescence of Aromatic Hydrocarbon Nanoparticles in an Aqueous Solution. J. Phys. Chem. C *113*, 11575–11578. https://doi.org/10.1021/jp901038h.
19. Wen, Y., Yang, G., Zhao, J., He, Y., Yuan, R., and Chen, S. (2022). An electrochemiluminescence biosensor based on morphology controlled iridium complex nanomaterials for SARS-CoV-2 nucleocapsid protein detection. Sensor. Actuator. B Chem. *371*, 132602. https://doi.org/10.1016/j.snb.2022.132602.
20. Li, X., Zha, M., Li, Y., Ni, J.S., Min, T., Kang, T., Yang, G., Tang, H., Li, K., and Jiang, X. (2020). Sub-10 nm Aggregation-Induced Emission Quantum Dots Assembled by Microfluidics for Enhanced Tumor Targeting and Reduced Retention in the Liver. Angew Chem. Int. Ed. Engl. *59*, 21899–21903. https://doi.org/10.1002/anie.202008564.
21. Middha, E., and Liu, B. (2020). Nanoparticles of Organic Electronic Materials for Biomedical Applications. ACS Nano *14*, 9228–9242. https://doi.org/10.1021/acsnano.0c02651.
22. Zhang, X., Wang, P., Nie, Y., and Ma, Q. (2021). Recent development of organic nanoemitter-based ECL sensing application. TrAC-Trend. Anal. Chem. *143*, 116410. https://doi.org/10.1016/j.trac.2021.116410.
23. Zhu, D., Zhang, Y., Bao, S., Wang, N., Yu, S., Luo, R., Ma, J., Ju, H., and Lei, J. (2021). Dual Intrareticular Oxidation of Mixed-Ligand Metal-Organic Frameworks for Stepwise Electrochemiluminescence. J. Am. Chem. Soc. *143*, 3049–3053. https://doi.org/10.1021/jacs.1c00001.
24. Carrara, S., Aliprandi, A., Hogan, C.F., and De Cola, L. (2017). Aggregation-Induced Electrochemiluminescence of Platinum(II) Complexes. J. Am. Chem. Soc. *139*, 14605–14610. https://doi.org/10.1021/jacs.7b07710.
25. Zhang, B., Kong, Y., Liu, H., Chen, B., Zhao, B., Luo, Y., Chen, L., Zhang, Y., Han, D., Zhao, Z., et al. (2021). Aggregation-induced delayed

Please cite this article in press as: Dai et al., Multicomponent supramolecular nanoaggregates with co-emissive electrochemiluminescence, Matter (2025), https://doi.org/10.1016/j.matt.2025.102056

fluorescence luminogens: the innovation of purely organic emitters for aqueous electrochemiluminescence. Chem. Sci. *12*, 13283–13291. https://doi.org/10.1039/d1sc02918e.

26. Wei, X., Zhu, M.J., Cheng, Z., Lee, M., Yan, H., Lu, C., and Xu, J.J. (2019). Aggregation-Induced Electrochemiluminescence of Carboranyl Carbazoles in Aqueous Media. Angew Chem. Int. Ed. Engl. *58*, 3162–3166. https://doi.org/10.1002/anie.201900283.
27. Liu, J.L., Zhang, J.Q., Tang, Z.L., Zhuo, Y., Chai, Y.Q., and Yuan, R. (2019). Near-infrared aggregation-induced enhanced electrochemiluminescence from tetraphenylethylene nanocrystals: a new generation of ECL emitters. Chem. Sci. *10*, 4497–4501. https://doi.org/10.1039/c9sc00084d.
28. Zhang, Y., Zhao, Y., Han, Z., Zhang, R., Du, P., Wu, Y., and Lu, X. (2020). Switching the Photoluminescence and Electrochemiluminescence of Liposoluble Porphyrin in Aqueous Phase by Molecular Regulation. Angew Chem. Int. Ed. Engl. *59*, 23261–23267. https://doi.org/10.1002/anie.202010216.
29. Liu, H., Wang, L., Gao, H., Qi, H., Gao, Q., and Zhang, C. (2017). Aggregation-Induced Enhanced Electrochemiluminescence from Organic Nanoparticles of Donor–Acceptor Based Coumarin Derivatives. ACS Appl. Mater. Interfaces *9*, 44324–44331. https://doi.org/10.1021/acsami.7b15434.
30. Omer, K.M., Ku, S.-Y., Cheng, J.-Z., Chou, S.-H., Wong, K.-T., and Bard, A.J. (2011). Electrochemistry and electrogenerated chemiluminescence of a spirobifluorene-based donor (triphenylamine)-acceptor (2,1,3-benzothiadiazole) molecule and its organic nanoparticles. J. Am. Chem. Soc. *133*, 5492–5499. https://doi.org/10.1021/ja2000825.
31. Han, T., Cao, Y., Wang, J., Jiao, J., Song, Y., Wang, L., Ma, C., Chen, H.Y., and Zhu, J.J. (2023). Crystallization-Induced Enhanced Electrochemiluminescence from a New Tris(bipyridine)ruthenium(II) Derivative. Adv. Funct. Mater. *33*, 2212394. https://doi.org/10.1002/adfm.202212394.
32. Shu, J., Han, Z., Zheng, T., Du, D., Zou, G., and Cui, H. (2017). Potential-resolved multicolor electrochemiluminescence of N-(4-Aminobutyl)-N-ethylisoluminol/tetra (4-carboxyphenyl) porphyrin/TiO2 nanoluminophores. Anal. Chem. *89*, 12636–12640. https://doi.org/10.1021/acs.analchem.7b04175.
33. Guo, W., Ding, H., Gu, C., Liu, Y., Jiang, X., Su, B., and Shao, Y. (2018). Potential-Resolved Multicolor Electrochemiluminescence for Multiplex Immunoassay in a Single Sample. J. Am. Chem. Soc. *140*, 15904–15915. https://doi.org/10.1021/jacs.8b09422.
34. Zhou, J., Nie, L., Zhang, B., and Zou, G. (2018). Spectrum-Resolved Triplex-Color Electrochemiluminescence Multiplexing Immunoassay with Highly-Passivated Nanocrystals as Tags. Anal. Chem. *90*, 12361–12365. https://doi.org/10.1021/acs.analchem.8b04424.
35. Geng, J., Zhu, Z., Qin, W., Ma, L., Hu, Y., Gurzadyan, G.G., Tang, B.Z., and Liu, B. (2014). Near-infrared fluorescence amplified organic nanoparticles with aggregation-induced emission characteristics for in vivo imaging. Nanoscale *6*, 939–945. https://doi.org/10.1039/c3nr04243j.
36. Xu, R., Zhang, P., Shen, Q., Zhou, Y., Wang, Z., Xu, Y., Meng, L., Dang, D., and Zhong Tang, B. (2023). AIE nanocrystals: Emerging nanolights with ultra-high brightness for biological application. Coord. Chem. Rev. *477*, 214944. https://doi.org/10.1016/j.ccr.2022.214944.
37. Li, C., Liu, Q., and Tao, S. (2022). Coemissive luminescent nanoparticles combining aggregation-induced emission and quenching dyes prepared in continuous flow. Nat. Commun. *13*, 6034. https://doi.org/10.1038/s41467-022-33857-x.
38. Marfin, Y.S., Banakova, E.A., Merkushev, D.A., Usoltsev, S.D., and Churakov, A.V. (2020). Effects of Concentration on Aggregation of BODIPY-Based Fluorescent Dyes Solution. J. Fluoresc. *30*, 1611–1621. https://doi.org/10.1007/s10895-020-02622-y.
39. Vu, T.T., Dvorko, M., Schmidt, E.Y., Audibert, J.-F., Retailleau, P., Trofimov, B.A., Pansu, R.B., Clavier, G., and Méallet-Renault, R. (2013). Understanding the Spectroscopic Properties and Aggregation Process of a New Emitting Boron Dipyrromethene (BODIPY). J. Phys. Chem. C *117*, 5373–5385. https://doi.org/10.1021/jp3097555.
40. Fabrizio, E.F., Prieto, I., and Bard, A.J. (2000). Hydrocarbon Cation Radical Formation by Reduction of Peroxydisulfate. J. Am. Chem. Soc. *122*, 4996–4997. https://doi.org/10.1021/ja000307y.
41. Hesari, M., Swanick, K.N., Lu, J.S., Whyte, R., Wang, S., and Ding, Z. (2015). Highly Efficient Dual-Color Electrochemiluminescence from BODIPY-Capped PbS Nanocrystals. J. Am. Chem. Soc. *137*, 11266–11269. https://doi.org/10.1021/jacs.5b07633.